Photoionization and electron-impact ionization of Kr^{3+}

M. Lu, G. Alna'washi, M. Habibi, M. F. Gharaibeh, and R. A. Phaneuf
Department of Physics, MS 220, University of Nevada, Reno, Nevada 89557-0058, USA

A. L. D. Kilcoyne, E. Levenson, and A. S. Schlachter
Advanced Light Source, Lawrence Berkeley National Laboratory, MS 7-100, Berkeley, California 94720-8225, USA

C. Cisneros and G. Hinojosa
Centro de Ciencias Físicas, Universidad Nacional Autónoma de México, Apartado Postal 6-96, Cuernavaca 62131, Mexcico
(Received 28 September 2006; published 1 December 2006)

Absolute photoionization cross sections for Kr^{3+} were measured in the energy range 39.05–143.2 eV for single ionization and 120.6–137.7 eV for double ionization. For comparison, an electron-impact single-ionization measurement was made in the energy range 43.1–179.1 eV and normalized to previously published absolute measurements. The Flexible Atomic Code and Cowan atomic structure codes were used to calculate energy levels, excitation energies and oscillator strengths for $3d \rightarrow np$, $3d \rightarrow nf$, and $4s \rightarrow np$ autoionizing transitions from the ground and metastable states. From the single-photoionization measurements, ionization thresholds of the $^2P^o_{3/2}$, $^2D^o_{5/2}$ metastable states and $^4S^o_{3/2}$ ground state were measured to be 46.62±0.02, 48.59±0.01, and 50.70±0.02 eV, nearly 2 eV lower than National Institute of Standards and Technology tabulated values. Within the experimental uncertainty, oscillator strengths determined from the photoionization measurements are in agreement with both calculations. Excitation-autoionization and resonant-excitation double-autoionization features are evident in the electron-impact ionization cross section.

DOI: 10.1103/PhysRevA.74.062701 PACS number(s): 32.80.Fb, 34.80.Dp, 32.80.Dz, 32.70.Cs

I. INTRODUCTION

Ionization processes involving multiply charged ions are important in laboratory and astrophysical plasmas. Krypton is an important element in controlled-fusion experiments. It is introduced as a diagnostic impurity for the central core plasma, as a source of electrons for studies of the edge plasma, and as a radiation "coolant" for diverters [1–5]. Ionization of the lower charge states of Kr ions by electrons and photons is important in models of the edge and divertor plasmas.

Electron-impact ionization of krypton ions has been studied extensively over the last few decades, both experimentally and theoretically. Ionization cross sections for Kr^{3+} were measured by Tinschert *et al.* [6] and by Gregory *et al.* [7]. Loch *et al.* [8] reported a complete theoretical study of the electron-impact single ionization of the krypton atom and its ions, calculating configuration-average distorted-wave cross sections and rate coefficients for all ionization stages. Although photoionization cross-section measurements on neutral krypton have been reported [9,10], only very recently has such data been reported for a krypton ion, Kr^{5+} [11]. Similarly, to our knowledge, published theoretical calculations of photoionization cross sections for Kr ions are not available.

This paper reports absolute cross-section measurements for single photoionization of Kr^{3+} in the energy range 39.05–143.2 eV, and for double photoionization in the energy range 120.6–137.7 eV. For comparison, in order to further elucidate the role of core-excited states, a detailed measurement of the energy dependence of the cross section for electron-impact single ionization of Kr^{3+} in the energy range 43.1–179.1 eV is also reported.

II. EXPERIMENT

Measurements of photoionization of Kr^{3+} ions were performed using the ion-photon-merged-beams endstation located at undulator beamline 10.0.1 of the Advanced Light Source (ALS). Details of the experimental setup and photoion spectroscopy technique have been reported [12], and only a brief description is presented here. Kr^{3+} ions were produced by a compact 10-GHz permanent-magnet electron cyclotron resonance (ECR) ion source and accelerated to 18 keV. After mass and charge-state selection by a dipole analyzing magnet, the Kr^{3+} ion beam was merged electrostatically with a monochromatized photon beam from an undulator. Two-dimensional spatial profiles of the merged ion and photon beams were measured by three translating-slit scanners located within the central interaction region of length 29.4 cm. A potential of +2 kV was applied to the interaction region to label Kr^{4+} or Kr^{5+} product ions produced therein with a different kinetic energy than those produced outside the region. A dipole analyzing magnet demerged the beams and separated the product ions from the primary Kr^{3+} beam, which was collected in a Faraday cup. The product Kr^{4+} or Kr^{5+} ions were directed to a single-particle detector and counted.

To record a photoionization spectrum, the relative yield of product ions was recorded as the photon energy was stepped. Absolute measurements of photoionization cross sections were also performed at a number of discrete photon energies to normalize the photoion-yield spectra. The total absolute uncertainty of the photoionization cross-section measurements is estimated to be ±23% at 90% confidence level, representing a quadrature sum of individual sources of uncertainty [12]. The major contributors are the beam profile measurements (±15%), determination of the beam overlap

integral (±10%), and the photon flux measurement (±10%).

The photon energy scale of the grating used for measurements below 75 eV was calibrated by comparing the well-known ionization thresholds of He^+ at 54.417 78 eV [13] and Ar^+ at 27.630 eV [13] to those measured using the endstation. The grating used at higher photon energies was calibrated with a gas cell using the Ar $(2p_{3/2}^{-1}3d)$ resonance in second order on the grating [reference energy =123.464(1) eV] [14] and S $(2p_{3/2}^{-1}4s)$ resonance in first order (reference energy=177.42 eV) and second order (reference energy=88.71 eV) [15]. The resulting uncertainty in the photon energy scale for the current measurements is estimated to be ±10 meV.

The electron-impact ionization measurement for Kr^{3+} was performed using an electron-ion crossed-beams apparatus at the Multicharged Ion Research Facility at the University of Nevada, Reno. This apparatus has been described in detail [16,17]. Kr^{3+} ions were produced in a 14.4-GHz ECR ion source and accelerated to 30 keV. After mass and charge-state selection by a dipole analyzing magnet, a collimated Kr^{3+} ion beam was crossed at right angles by an electron beam [18]. The Kr^{4+} product ions were separated from the parent Kr^{3+} ion beam by a 90° dipole analyzing magnet and counted by a single-particle detector. The primary Kr^{3+} ion beam was collected in a Faraday cup. The electron gun can be translated mechanically to optimize the spatial overlap of the electron and ion beams. A separate measurement of the Kr^{4+} background produced by collisions with residual gas was made at an electron gun position where the two beams did not overlap.

An electron-impact ionization spectrum was obtained by recording the relative yield of Kr^{4+} product ions as the electron beam energy was stepped, and then subtracting a background spectrum obtained when the beams were not crossed. Measurement of the energy dependence of the cross section was made using energy steps as small as 73 meV at optimum beam overlap. The high-statistical-precision spectrum was obtained by scanning over the same electron beam energy range from several tens to hundreds of sweeps, depending on the count rate (typically 10 kHz) and signal-to-background ratio.

III. ATOMIC STRUCTURE CALCULATIONS

As a guide in identifying structures in the measurements, calculations were performed using the Flexible Atomic Code (FAC) [19] and Cowan [20] Hartree-Fock atomic structure code. Configuration-interaction effects are taken into account by the Cowan code calculation, which is based on LS coupling. The FAC code is fully relativistic based on the Dirac equation, and the fine-structure of core-excited autoionizing states that are omitted in LS coupling calculations are treated naturally [21].

In the calculation of $4s \rightarrow np$ excitations, $4s^24p^3$ was selected as the initial configuration and $4s4p^3np$ $(5 \leqslant n \leqslant 10)$ as the final configuration. For $3d \rightarrow np$ and $3d \rightarrow nf$ core electron excitations, $3d^{10}4s^24p^3$ was chosen as the initial configuration, and $3d^94s^24p^3np$ $(4 \leqslant n \leqslant 9)$, $3d^94s^24p^3nf$ $(4 \leqslant n \leqslant 20)$ as the final configurations, respectively. The ranges of principal quantum numbers for the calculations were chosen to overlap the energy ranges of the measurements. To determine the contributions of these states to ionization, the decay rates for these final states were also calculated. The Auger rates were found to be much larger than the radiative rates. Therefore, absorption oscillator strengths may be derived from the measured photoionization resonance strengths.

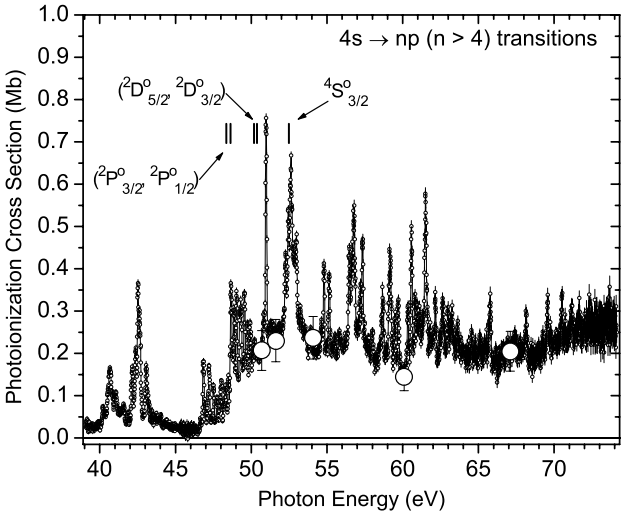

FIG. 1. Apparent absolute single-photoionization cross section of Kr^{3+} measured with a photon energy resolution of 100 meV, showing $4s \rightarrow np$ transitions. The large empty circles with error bars show the absolute cross section measurements with their uncertainties. The vertical bars indicate the ionization thresholds for the $^2P^0_{3/2}$, $^2P^0_{1/2}$, $^2D^0_{5/2}$ and $^2D^0_{3/2}$ metastable states and the $^4S^0_{3/2}$ ground state tabulated in the NIST database.

IV. EXPERIMENTAL RESULTS AND ANALYSIS

A. Photoionization of Kr^{3+}

The $^{84}Kr^{3+}$ ion beam was accompanied by small undetermined fractions of N_2^+ and CO^+ ions, which have the same charge-to-mass ratio. However, the presence of these contaminant ions in the primary beam had no effect on the measured relative yield of $^{84}Kr^{4+}$ or $^{84}Kr^{5+}$ products, since their ionization or fragmentation products do not reach the photoion detector when the charge analyzer is set to detect $^{84}Kr^{4+}$ or $^{84}Kr^{5+}$ ions. The effect was therefore a dilution of the primary ion beam, affecting only the normalization to the primary ion beam current. Because the isotopic abundance of ^{84}Kr is 56.9% compared to 17.4% for the next most abundant isotope (^{86}Kr), the relative photoion-yield spectrum was measured using $^{84}Kr^{3+}$ as a primary ion beam, improving the signal count rate and statistical precision of the data. The spectrum was subsequently normalized to absolute cross-section measurements performed using an $^{86}Kr^{3+}$ ion beam, whose purity could be assured.

1. Near-threshold region and $4s \rightarrow np$ excitation-autoionization

Figure 1 shows the absolute single-photoionization cross section of Kr^{3+} as a function of photon energy in the energy

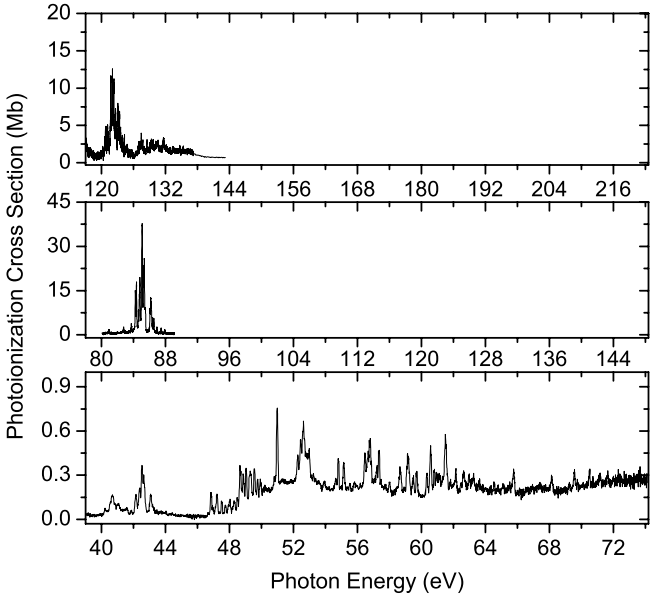

FIG. 2. Apparent single-photoionization cross section of Kr^{3+} from Fig. 1 (lower panel). The middle and upper panels show similar photoionization measurements made at twice and three times the photon energy. Note the large difference in cross-section scales in these three energy ranges and the correspondence of resonance features below 46 eV in the lower panel, indicating contributions due to second and third order radiation in the photon beam.

range 39.05–74.11 eV at a photon energy resolution of 100 meV. The cross section contains a large number of resonance features. The ground-state configuration of Kr^{3+} is $3d^{10}4s^24p^3$ with $^4S^0_{3/2}$ ground state and $^2D^0_{3/2}$, $^2D^0_{5/2}$, $^2P^0_{1/2}$, and $^2P^0_{3/2}$ metastable states. The ionization thresholds tabulated in the National Institute of Standard and Technology (NIST) atomic spectra database [13] for these five states are 52.49, 50.38, 50.18, 48.64, and 48.35 eV, respectively. Resonance structure above the ionization threshold of the highest-lying $^2P^0_{3/2}$ metastable state is attributed to $4s \rightarrow np$ transitions. It is difficult to assign specific transitions to the individual resonances because there are many transitions in each energy band and the different transition bands overlap.

Below the ionization threshold of the highest-lying $^2P^0_{3/2}$ metastable state (48.35 eV in the NIST database), a number of resonance structures are evident in the measurement. As shown in Fig. 2, features in the range of twice the energy of the $4s \rightarrow np$ spectrum due to $3d \rightarrow 4p$ transitions and three times the energy due to $3d \rightarrow np$ $(n > 4)$ and $3d \rightarrow nf$ $(n > 3)$ transitions have large cross sections, as discussed later. The comparison indicates that the resonance features between 39.05 and 46 eV are due to small components $(\sim 1\%)$ of second and third order radiation in the photon beam [22].

The origin of additional resonance features in the energy range 46–48.35 eV is less clear. To check whether they are produced by Kr^{3+} ions, the photoion yield for the $^{86}Kr^{3+}$ isotope in the photon energy range 46.25–50.30 eV was measured at an energy resolution of 100 meV. The result is compared in Fig. 3 with the $^{84}Kr^{3+}$ measurement made in the same energy range with the same energy resolution. Two

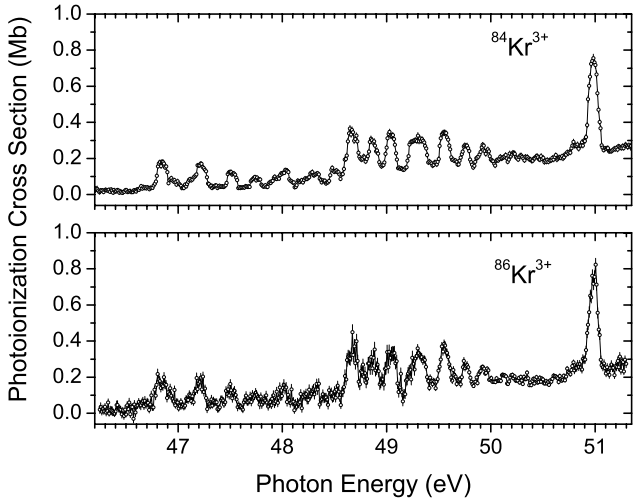

FIG. 3. Comparison of single-photoionization cross-section measurements at the same photon energy resolution (100 meV) made with $^{86}Kr^{3+}$ and $^{84}Kr^{3+}$.

spectra are identical, verifying that the resonance structures in the photon energy range 46–48.35 eV were produced by the Kr^{3+} ions and not an impurity in the ion beam. This led to a suspicion that the ionization threshold energies tabulated in the NIST atomic database might be inaccurate, and to further measurements at higher photon energy resolution.

Figure 4 presents a blowup of the near-threshold energy region in Fig. 1. Three prominent level shifts in the photoionization cross section are evident near 46.62, 48.6, and 50.7 eV, respectively with the measured cross section close to zero at 46.5 eV. These together suggest that the ionization thresholds for the $^2P^0_{3/2}$, $^2D^0_{5/2}$ metastable states and $^4S^0_{3/2}$ ground state of Kr^{3+} are 46.62, 48.6, and 50.7 eV, respectively. The small nonzero cross section below 46.5 eV is attributed to high-order radiation as discussed above. Figure 5 shows the photoion-yield spectrum for Kr^{3+} in the photon

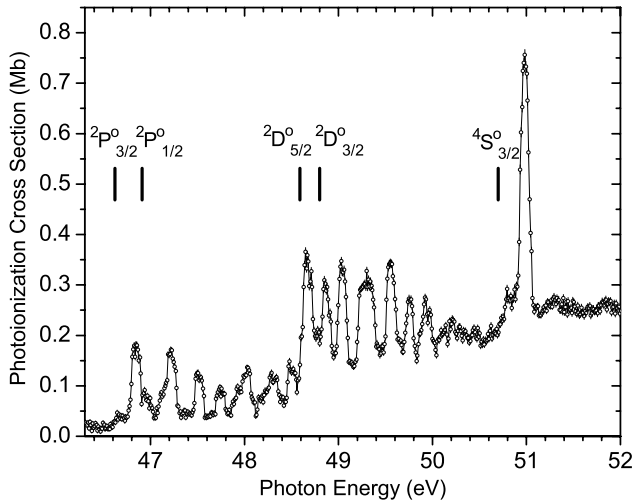

FIG. 4. Blowup of the threshold region of Fig. 1. The vertical bars indicate the corrected ionization thresholds for the $^2P^0_{3/2}$, $^2P^0_{1/2}$, $^2D^0_{5/2}$, and $^2D^0_{3/2}$ metastable states and the $^4S^0_{3/2}$ ground state. See text for details.

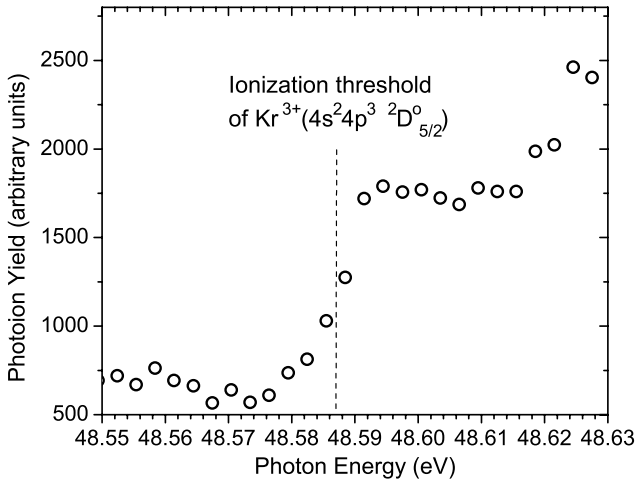

FIG. 5. Photoion yield for Kr^{3+} as a function of the photon energy measured at higher resolution (30 meV), indicating that the ionization threshold for the $^2D^0_{5/2}$ metastable state is 48.59±0.01 eV.

energy range 48.55–48.63 eV at a higher energy resolution of 30 meV, clearly resolving the threshold step from the nearby resonance feature. A more accurate ionization potential of the $^2D^0_{5/2}$ metastable state is determined to be 48.59±0.01 eV. The ionization thresholds of the $^2P^0_{1/2}$ and $^2D^0_{3/2}$ metastable states are not as evident from these measurements because of nearby resonance structures. Using these experimental values and assuming that the fine-structure energy splittings of the $^2D^0$ and $^2P^0$ states tabulated in the NIST database are correct, the five ionization thresholds within the ground-state configuration of Kr^{3+} were determined as indicated in Fig. 4. The FAC and Cowan codes were also used to calculate the ionization thresholds for these states. The calculation results, the data from the NIST database, and the values determined from the present measurement are compared in Table I. It is noteworthy that differences between the values derived from the present measurements and the NIST-tabulated values are nearly 2 eV.

The integrated oscillator strength for $4s \rightarrow np$ transitions were obtained using the formula [23]

TABLE I. Ionization thresholds (eV) of Kr^{3+} ($3d^{10}4s^24p^3$).

State	FAC	Cowan	NIST	Experiment
$^4S^0_{3/2}$	49.98	50.64	52.49	50.70±0.02
$^2D^0_{3/2}$	47.40	48.46	50.38	48.79[a]
$^2D^0_{5/2}$	47.20	48.28	50.18	48.59±0.01
$^2P^0_{1/2}$	45.40	46.75	48.64	46.91[a]
$^2P^0_{3/2}$	45.11	46.49	48.35	46.62±0.02

[a]Estimated assuming that the fine-structure splittings in the NIST database are correct.

$$f = (9.11 \times 10^{-3}) \int_{E_1}^{E_2} \sigma(E) dE,$$

where f is a dimensionless quantity, $\sigma(E)$ is the cross section in Mb, E is the photon energy in eV, and E_1 and E_2 are the energy limits of the range for which the oscillator strength is to be calculated. The energy interval for the integration is 46.7 to 72.1 eV and the result is presented in Table II. The oscillator strengths calculated for those same transitions using the FAC and Cowan codes, and for the corresponding energy ranges for the transitions are also tabulated. For all comparisons between calculations and experiment, a statistical admixture within the ground-state configuration of the $^4S^0_{3/2}(1/5)$ ground state and $^2D^0_{3/2}(1/5)$, $^2D^0_{5/2}(3/10)$, $^2P^0_{1/2}(1/10)$ and $^2P^0_{3/2}(1/5)$, metastable states was assumed to represent the distribution of initial states in the ion beam. For $4s \rightarrow np$ transitions, the oscillator strengths were calculated up to $n=10$.

The two calculations give significantly different oscillator strengths for $4s \rightarrow np$ transitions, with the experimental value falling between them. Note that the calculated oscillator strengths for $4s \rightarrow 5p$ transitions are smaller than those for $4s \rightarrow 6p$ transitions in both calculations. This is because not all of the $4s \rightarrow 5p$ transitions lie above the ionization threshold of the highest-lying $^2P^0_{3/2}$ metastable state.

2. 3d→np, nf excitation autoionization

Figure 6 shows the absolute single-photoionization cross section of Kr^{3+} as a function of photon energy in the energy

TABLE II. Comparison of integrated oscillator strengths for $4s \rightarrow np$ transitions determined from experiment with calculated values for $5 \leqslant n \leqslant 10$.

Transition	Oscillator strengths (Expt.)	Oscillator strengths (FAC)	Oscillator strengths (Cowan)	Energy band (eV) (FAC)	Energy band (eV) (Cowan)	Energy range (eV) (Expt.)
$4s \rightarrow 5p$		0.00623	0.01446	34.5–55.7	36.4–54.6	
$4s \rightarrow 6p$		0.01142	0.01978	43.6–63.9	45.8–63.4	
$4s \rightarrow 7p$		0.00633	0.00988	47.8–67.9	50.1–67.5	
$4s \rightarrow 8p$		0.00380	0.00568	50.2–70.2	52.4–69.8	
$4s \rightarrow 9p$		0.00245	0.00357	51.6–71.6	53.8–71.2	
$4s \rightarrow 10p$		0.00167	0.00239	52.6–72.5	54.8–72.1	
Sum	0.042±0.010	0.03190	0.05576			46.7–72.1

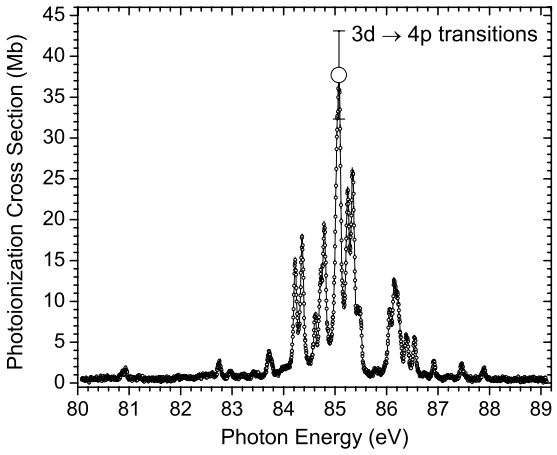

FIG. 6. Absolute single-photoionization cross section in the energy range of $3d \rightarrow 4p$ transitions in Kr^{3+} measured with an energy resolution of 50 meV. The large open circle with error bar shows an absolute cross-section measurement made at the same energy resolution, with its estimated uncertainty.

range 80.1–89.1 eV. The photon energy resolution in this measurement was 50 meV. Compared to the small nonresonant direct photoionization contribution, the resonance structures dominate the cross section in this photon energy range and are attributed to $3d \rightarrow 4p$ transitions.

To compare the measurement with the two calculations for $3d \rightarrow 4p$ transitions, the theoretical results were convoluted with a Gaussian profile accounting for the instrumental resolution function [50 meV full width at half maximum (FWHM)], keeping the total calculated oscillator strength the same. The comparison is presented in Fig. 7. The theoretical cross section is brought into reasonable agreement with the experiment by shifting the calculated energies by +0.81 eV for the Cowan code result and by +1.56 eV for the FAC code result.

Figure 8 shows the absolute single-photoionization cross section measurement for Kr^{3+} in the photon energy

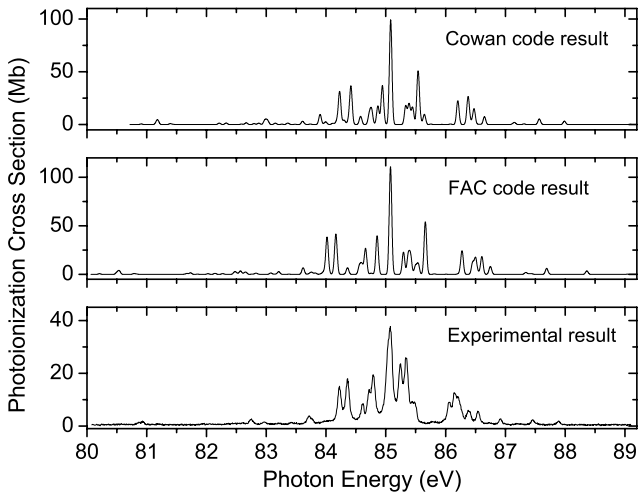

FIG. 7. Comparison of absolute cross-section measurements for single photoionization of Kr^{3+} with calculated values, shifted by +0.81 eV for Cowan code result and by +1.56 eV for FAC code result.

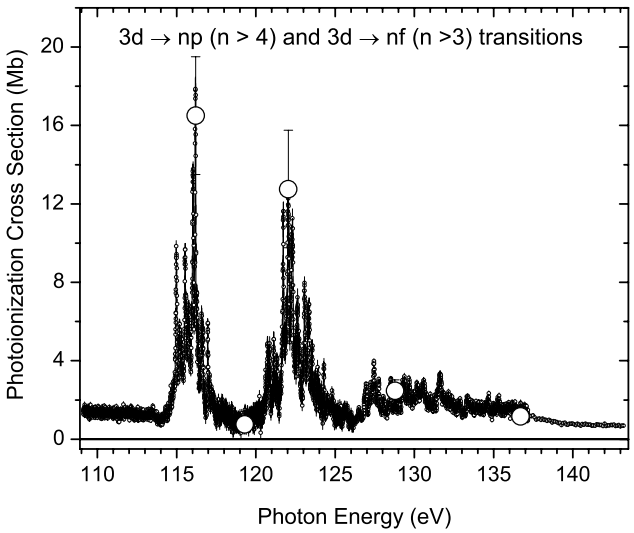

FIG. 8. Single-photoionization cross section in the energy range of the $3d \rightarrow np$ $(n>4)$ and $3d \rightarrow nf$ $(n>3)$ transitions in Kr^{3+} measured with an energy resolution of 50 meV in the energy range 109.1–137.2 eV, and a resolution of 200 meV in the energy range 137.2–143.2 eV. The large open circles with error bars show individual absolute cross-section measurements and their uncertainties.

109.1–143.2 eV. The region of the spectrum below 137.2 eV was measured at a resolution of 50 meV with 5 meV steps, while the higher-energy region was measured at a resolution of 200 meV with 100 meV energy steps due to its lack of structure. The resonance features that dominate the cross section are attributed to $3d \rightarrow np$ $(n>4)$ and $3d \rightarrow nf$ $(n>3)$ transitions. It is difficult to assign the individual resonances because there are many transitions within each band and the different transition bands overlap in energy.

The oscillator strengths and the corresponding energy bands for $3d \rightarrow np$ $(4 \leqslant n \leqslant 9)$ and $3d \rightarrow nf$ $(4 \leqslant n \leqslant 20)$ transitions were calculated using FAC and Cowan codes. The results are presented in Table III along with oscillator strengths determined from the measurements and the corresponding energy intervals for the integrations. The experimental oscillator strengths for $3d \rightarrow 4p$ transitions and $3d \rightarrow np$, $3d \rightarrow nf$ transitions agree with both the theoretical calculations, well within the experimental uncertainty of ±23%.

3. Double photoionization

Figure 9 shows the absolute double-photoionization cross section of Kr^{3+} in the energy range 120.6–137.7 eV measured with a resolution 50 meV. For comparison, the single-photoionization cross section of Kr^{3+} measured in the same energy range with the same resolution is also shown. The double-photoionization resonance features correspond to those for single photoionization, indicating excitation of the same intermediate excited states, but followed by decay along different pathways. The resonance structure in the double-photoionization spectrum is attributed to $3d \rightarrow np$, nf excitation followed by double autoionization, in which two Auger electrons are emitted sequentially. A possible process is

TABLE III. Experimental and calculated oscillator strengths and the corresponding energy intervals for $3d \rightarrow np$ and $3d \rightarrow nf$ transitions.

Transition	Oscillator strengths (Expt.)	Oscillator strengths (FAC)	Oscillator strengths (Cowan)	Energy band (eV) (FAC)	Energy band (eV) (Cowan)	Energy range (eV) (Expt.)
$3d \rightarrow 4p$	0.242±0.056	0.2775	0.2521	78.7–88.9	80.1–90.7	80.1–89.1
$3d \rightarrow 5p$		0.0767	0.0520	107.5–120.9	109.7–121.2	
$3d \rightarrow 6p$		0.0279	0.0201	116.8–129.3	119.3–130.2	
$3d \rightarrow 7p$		0.0136	0.0100	121.1–133.4	123.6–134.5	
$3d \rightarrow 8p$		0.0077	0.0056	123.4–135.8	125.9–136.8	
$3d \rightarrow 9p$		0.0048	0.0036	124.8–137.2	127.3–138.2	
$3d \rightarrow 4f$		0.1285	0.1266	114.5–127.6	116.7–128.2	
$3d \rightarrow 5f$		0.0995	0.0979	119.8–132.3	122.1–133.2	
$3d \rightarrow 6f$		0.0675	0.0657	122.4–135.0	125.1–136.0	
$3d \rightarrow 7f$		0.0460	0.0443	124.2–136.7	126.8–137.7	
$3d \rightarrow 8f$		0.0322	0.0309	125.3–137.8	127.9–138.8	
$3d \rightarrow 9f$		0.0232	0.0222	126.1–138.5	128.6–139.6	
$3d \rightarrow 10f$		0.0173	0.0164	126.6–139.1	129.2–140.1	
$3d \rightarrow 11f$		0.0131	0.0124	127.0–139.5	129.6–140.5	
$3d \rightarrow 12f$		0.0102	0.0097	127.3–139.8	129.9–140.8	
$3d \rightarrow 13f$		0.0081	0.0076	127.6–140.0	130.1–141.1	
$3d \rightarrow 14f$		0.0065	0.0061	127.7–140.2	130.3–141.2	
$3d \rightarrow 15f$		0.0053	0.0050	127.9–140.3	130.4–141.4	
$3d \rightarrow 16f$		0.0044	0.0041	128.0–140.4	130.5–141.5	
$3d \rightarrow 17f$		0.0037	0.0034	128.1–140.5	130.6–141.3	
$3d \rightarrow 18f$		0.0031	0.0029	128.2–140.6	130.7–141.4	
$3d \rightarrow 19f$		0.0026	0.0025	128.3–140.7	130.8–141.5	
$3d \rightarrow 20f$		0.0023	0.0021	128.3–140.7	130.9–141.5	
$3d \rightarrow np, nf$ $(n \geqslant 4)$	0.849±0.195	0.8817	0.8032	78.7–140.7	80.1–141.5	80.1–143.2

$$\begin{aligned} \mathrm{Kr}^{3+}(3d^{10}4s^24p^3) + \gamma &\rightarrow \mathrm{Kr}^{3+}(3d^94s^24p^3np,nf) \\ &\rightarrow \mathrm{Kr}^{4+}(3d^{10}4s4p^3) + e^- \\ &\rightarrow \mathrm{Kr}^{5+}(3d^{10}4s^24p) + 2e^-. \end{aligned} \quad (1)$$

This process competes with that leading to single ionization,

$$\begin{aligned} \mathrm{Kr}^{3+}(3d^{10}4s^24p^3) + \gamma &\rightarrow \mathrm{Kr}^{3+}(3d^94s^24p^3np,nf) \\ &\rightarrow \mathrm{Kr}^{4+}(3d^{10}4s^24p^2) + e^-. \end{aligned} \quad (2)$$

The main difference between processes (1) and (2) is the participation of a $4s$ electron in process (1), creating an additional inner-shell vacancy that permits emission of a second Auger electron.

A useful parameter in plasma physics modeling is the ratio of double to single photoionization cross sections. Figure 10 shows that this ratio for Kr^{3+} increases with photon energy in the range 120.6–137.2 eV. Above 132 eV, the ratio is consistently greater than one, indicating that the intermediate excited states favor decay via double rather than single autoionization as the photon energy increases.

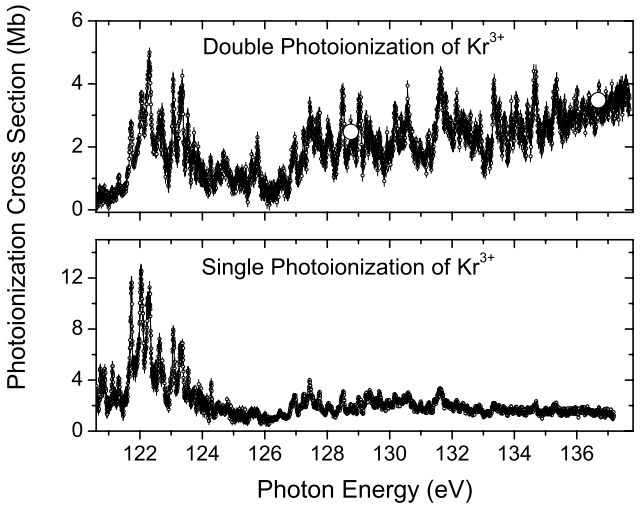

FIG. 9. Comparison of the absolute double-photoionization cross section for the $3d \rightarrow np$ $(n>4)$ and $3d \rightarrow nf$ $(n>3)$ transitions in Kr^{3+} measured at an energy resolution of 50 meV in the energy range 120.6–137.7 eV with the measured single-photoionization cross section for the same transitions at the same energy resolution. The large open circles indicate individual absolute cross section measurements that were used to normalize the spectrum.

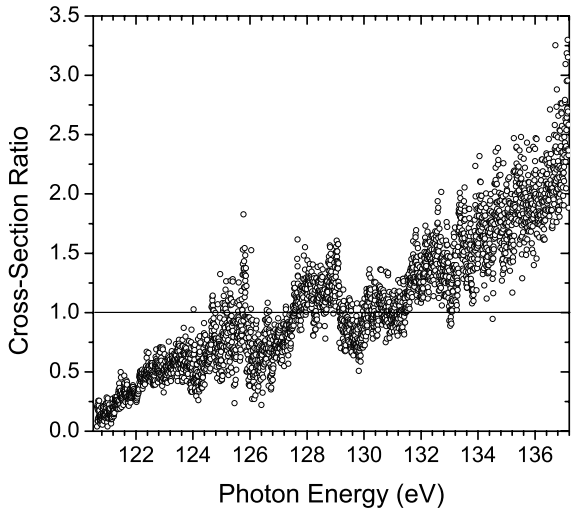

FIG. 10. Ratio of double to single photoionization cross sections of Kr^{3+} as a function of the photon energy in the energy range 120.6–137.2 eV.

B. Electron-impact ionization of Kr^{3+}

The atomic structure of Kr^{3+} ions is characterized by an Ar-like core with a $3d^{10}4s^24p^3$ outer-shell configuration. The configuration-average ionization potentials calculated for these subshells using the Cowan code are 136.66, 66.65, and 49.80 eV, respectively and are presented in Table IV.

The measured electron-impact single-ionization cross section of Kr^{3+} in the energy range 43.1–179.1 eV is shown in Fig. 11. The electron energy resolution is approximately 1 eV. The relative yield of Kr^{4+} product ions was measured in a fine energy-scanning mode and normalized arbitrarily to the absolute cross-section measurements of Tinschert *et al.* [6]. Also shown in Fig. 11 are absolute measurements of Gregory *et al.* [7]. Configuration-average distorted-wave theoretical calculations by Loch *et al.* [8], both for direct ionization and including excitation-autoionization (EA) contributions, are presented for comparison, as is the prediction of the single-parameter Lotz semiempirical formula [24] for direct single ionization of Kr^{3+},

$$\sigma(E) = 4.5 \times 10^{-14} \sum_j \frac{r_j}{I_j E} \ln(E/I_j),$$

where the cross section σ at a collision energy E (in eV) is given in cm^2, r_j is the number of electrons in subshell j, and I_j is the ionization energy (in eV) for electrons in that subshell. Direct ionization of the $3d$ subshell has not been included in the theoretical data or the Lotz formula data presented, since subsequent autoionization would be expected to lead predominantly to double ionization of Kr^{3+}. It should be noted that both the theoretical calculations and Lotz formula represent ionization from the ground state of Kr^{3+} only (I.P.=50.7 eV), whereas the measurements near threshold indicate substantial population of the metastable states (lowest I.P.=46.6 eV, see Table I), as was observed in the photoionization measurements. Part of the underestimation of the ionization cross section by the theory at energies below the major EA thresholds is likely due to contributions from the resonant-excitation double-autoionization (REDA) process, evidenced by resonance structure in the data as discussed below.

TABLE IV. Calculated configuration-average ionization and excitation energies for Kr^{3+}.

Subshell	Ionization potential (eV)
$4p$	49.80
$4s$	66.65
$3d$	136.66
Transition	Excitation energy (eV)
$3d \rightarrow 4p$	84.01
$3d \rightarrow 4d$	107.64
$3d \rightarrow 4f$	122.10
$3d \rightarrow 5p$	115.13
$3d \rightarrow 5d$	121.87
$3d \rightarrow 5f$	127.42
$3d \rightarrow 6p$	124.45
$3d \rightarrow 6d$	127.45
$3d \rightarrow 6f$	130.28

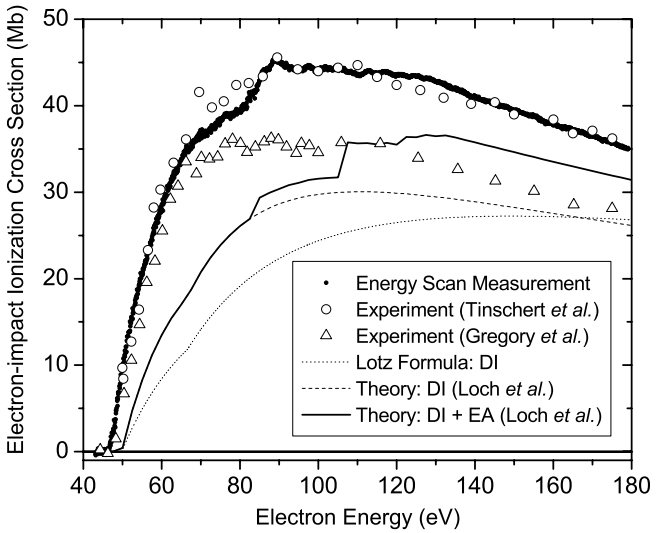

FIG. 11. Energy-scan measurement of the cross section for electron-impact ionization of Kr^{3+} (small dots) normalized to the absolute measurement of Tinschert *et al.* [6] (open circles). The experimental energy resolution is approximately 1 eV. Triangles indicate absolute measurements of Gregory *et al.* [7]. The dotted-line curve is the semiempirical Lotz formula prediction for the direct ionization cross section. The dashed and solid curves are the distorted-wave direct ionization and direct ionization (DI) plus excitation-autoionization (EA) calculations of Loch *et al.* [8].

1. $4s \rightarrow nl$ excitation-autoionization

Figure 12(a) presents the electron-impact single-ionization cross section as a function of electron energy for Kr^{3+} near the ionization threshold. For comparison, the single-photoionization measurements in the same energy

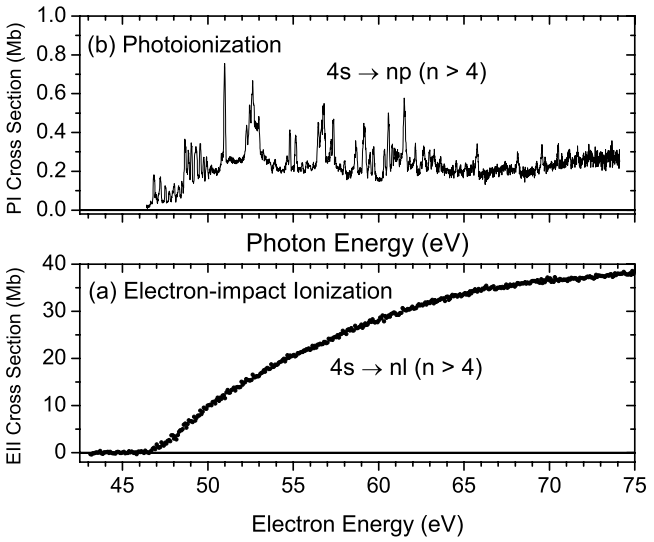

FIG. 12. Comparison of electron-impact single-ionization cross-section measurements for Kr^{3+} (a) with the single-photoionization cross-section measurements (b) in the energy range 43.1 to 75 eV.

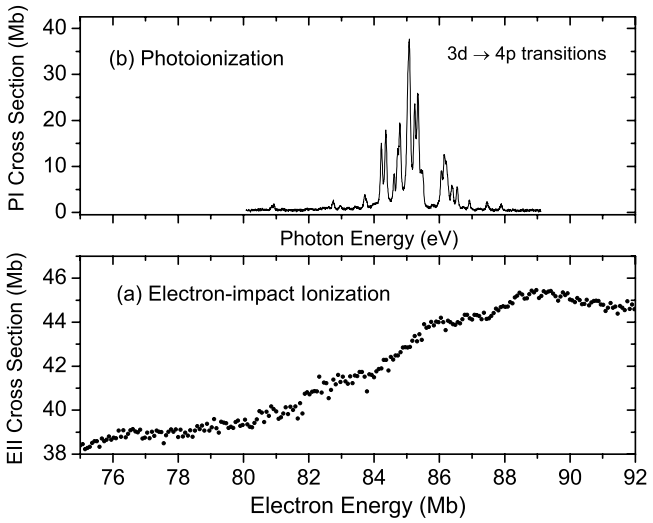

FIG. 13. Comparison of electron-impact single-ionization cross-section measurements for Kr^{3+} (a) with the single-photoionization cross-section measurements (b) in the energy range 75 to 92 eV.

range are shown in Fig. 12(b). The observed electron-impact ionization threshold near 46.6 eV indicates that the parent Kr^{3+} ion beam contained ions in the $3d^{10}4s^24p^3\ ^2P^o_{3/2}$ metastable state, consistent with the photoionization measurement. The cross section rises more steeply than predicted by the Lotz formula in this energy range, suggesting a series of excitation-autoionization onsets due to $4s \rightarrow nl$ transitions. It is noted that $4s \rightarrow np$ $(n > 4)$ transitions are prominent in the single-photoionization cross section in this photon energy range. However, apparent enhancement of the electron-impact ionization cross section due to $4s \rightarrow nl$ transitions just above the ionization threshold is significant, whereas the corresponding $4s \rightarrow np$ photoionization cross section is relatively small. A possible explanation is that electric-dipole-forbidden transitions contribute significantly to electron-impact ionization, but are absent in photoionization. Distinct steps for individual transitions are not evident in electron-impact ionization because there are many transitions in each band and the different transition bands overlap.

2. $3d \rightarrow nl$ excitation-autoionization

Figure 13(a) shows the electron-impact single-ionization cross section of Kr^{3+} in the energy range 80.2–154.3 eV. Again, the single-photoionization measurements in the same energy range are shown in Fig. 13(b). A change in slope is evident in the electron-impact ionization cross section near 80 eV. The comparison suggests that this change is due to the onset of $3d \rightarrow 4p$ excitation autoionization. Possible weak resonances in the electron-impact ionization cross section near 86 eV may be due to the REDA process [25] involving the $3d^94s^24p^4nl$ intermediate autoionizing state of Kr^{2+} that decays by sequential ejection of two electrons. The $3d \rightarrow 4p$ transitions that contribute significantly to the photoionization cross section are also evident in the electron-impact ionization cross section.

Figure 14(a) shows the electron-impact single-ionization cross section of Kr^{3+} measured in the energy range 92–138 eV. The single-photoionization measurements in the same energy range are also shown in Fig. 13(b). The calculated configuration-average excitation and ionization energies of $3d \rightarrow nl$ transitions are marked by the vertical lines and presented in Table IV. The calculated energy band for $3d \rightarrow 4d$ transitions is from 100 to 118 eV. The distinct change in slope in the electron-impact ionization cross section at 110 eV is attributed to electric-dipole forbidden $3d \rightarrow 4d$ transitions, which are unobservable in the photoionization spectrum. This energy is higher than the calculated configuration-average $3d \rightarrow 4d$ excitation energy of 107.64 eV, which is expected to be accurate within approximately ±1 eV. This suggests that the low-energy transitions within the $3d \rightarrow 4d$ band are weak. Theoretical calculations by Gorczyca *et al.* [26] for Kr^{4+} and Kr^{5+} indicated that $3d \rightarrow 4d$ transitions contribute a large cross section to electron-

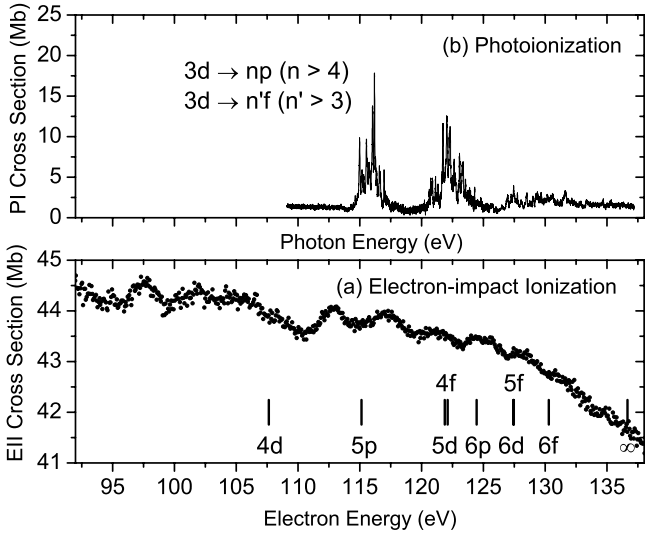

FIG. 14. Comparison of electron-impact single-ionization cross-section measurements for Kr^{3+} (a) with the single-photoionization cross-section measurements (b) in the energy range 92 to 138 eV.

impact ionization, which is consistent with the present Kr^{3+} measurement. A number of resonance features are evident between 92 and 110 eV. These features lie above the $3d \rightarrow 4p$ transition band and below the $3d \rightarrow 4d$ transition band, suggesting that they are most likely produced by the REDA process, as discussed above. In this case one $3d$ electron is excited to a $4d$ orbital instead of a $4p$ orbital.

Another distinct step near 115 eV in the electron-impact ionization cross section is most likely due to $3d \rightarrow 5p$ excitation-autoionization. Steps at about 120 and 123.3 eV are attributed to $3d \rightarrow 5d$, $3d \rightarrow 4f$, and $3d \rightarrow 6p$ transitions. Another step near 127 eV may be due to $3d \rightarrow 6d$ and $3d \rightarrow 5f$ transitions. Above 129 eV, the ionization cross section is relatively smooth, suggesting that the excitation-autoionization cross sections become smaller for $3d \rightarrow nl$ transitions as n increases and the different transitions overlap in energy.

V. SUMMARY AND CONCLUSIONS

Absolute cross sections were measured for single photoionization of Kr^{3+} in the photon energy range 39.05–143.2 eV and for double photoionization in the energy range 120.6–137.7 eV. The detailed energy dependence of the cross section for electron-impact single ionization was also measured in the electron energy range 43.1–179.1 eV.

Ionization thresholds of the $^2P^o_{3/2}$ and $^2D^o_{5/2}$ metastable states and $^4S^o_{3/2}$ ground state were measured to be 46.62 ± 0.02, 48.59 ± 0.01, and 50.70 ± 0.02 eV, nearly 2 eV lower than NIST-tabulated values. The resonance features in the single-photoionization cross section in the photon energy 46.62–72.1 eV are attributed to excitation-autoionization of $4s \rightarrow np$ $(n > 4)$ transitions. In the photon energy range 80.1–143.2 eV, the absolute single-photoionization cross section is dominated by excitation of an inner-shell $3d$ electron into np and nf $(n \geq 4)$ orbitals. The double-photoionization resonance features correspond to those observed in single photoionization, indicating that they are due to excitation of the same intermediate excited states followed by decay along different pathways. The ratio of double to single photoionization cross sections generally increases with photon energy and is greater than one above 132 eV.

The FAC and Cowan Hartree-Fock atomic structure codes were used to calculate energy levels, excitation and ionization energies, and oscillator strengths for autoionizing transitions from the ground state ($3d^{10}4s^24p^3\ ^4S^o_{3/2}$) and metastable states ($3d^{10}4s^24p^3\ ^2D^o_{3/2}$, $^2D^o_{5/2}$, $^2P^o_{1/2}$, and $^2P^o_{3/2}$) of Kr^{3+}. The theoretical calculations are brought into agreement with the single-photoionization measurement for $3d \rightarrow 4p$ excitation-autoionization by shifting the calculated energies by +0.81 eV for the Cowan code result and by +1.56 eV for the FAC code result. Within the experimental uncertainty, the measured oscillator strengths are in agreement with both theoretical calculations.

Detailed energy-scan measurements indicate that the electron-impact single-ionization cross section for Kr^{3+} in the electron energy range from the ionization threshold up to 72 eV is dominated by $4s \rightarrow nl$ excitation-autoionization processes. In the electron energy range 80.1–143.2 eV, the $3d \rightarrow nd$ $(n \geq 4)$ electric-dipole forbidden transitions contribute significantly to the electron-impact ionization cross section. Several resonant-excitation double-autoionization features, which are related to the $3d \rightarrow 4p$, $4d$ excitations, are identified in the electron-impact ionization measurement.

ACKNOWLEDGMENTS

The authors are grateful to Bruce Rude for expert technical assistance. This research was supported by the U.S. Department of Energy under Grant No. DE-FG02-03ER15424 and Contract No. DE-AC03-76SF-00098. C.C. and G.H. acknowledge support from DGAPA-UNAM and from DGAPA-UNAM IN-115405, México, respectively.

[1] K. Widmann, P. Beiersdorfer, V. Decaux, S. R. Elliott, D. Knapp, A. Osterheld, M. Bitter, and A. Smith, Rev. Sci. Instrum. **66**, 761 (1995).

[2] K. W. Hill, S. D. Scott, M. Bell, R. Budny, C. E. Bush, R. E. H. Clark, B. Denne-Hinnov, D. R. Ernst, G. W. Hammett, D. R. Mikkelsen, D. Mueller, J. Ongena, H. K. Park, A. T. Ramsey, E. J. Synakowski, G. Taylor, M. C. Zarnstorff, *and the TFTR Group*, Phys. Plasmas **6**, 877 (1999).

[3] M. Bitter, H. Hsuan, C. Bush, S. Cohen, C. J. Cummings, B. Grek, K. W. Hill, J. Schivell, M. Zarnstorff, P. Beiersdorfer, A. Osterheld, A. Smith, and B. Fraenkel, Phys. Rev. Lett. **71**, 1007 (1993).

[4] R. Radtke, C. Biedermann, T. Fuchs, G. Fussmann, and P. Beiersdorfer, Phys. Rev. E **61**, 1966 (2000).

[5] H. Chen, P. Beiersdorfer, K. B. Fournier, and E. Träbert, Phys. Rev. E **65**, 056401 (2002).

[6] K. Tinschert, A. Müller, G. Hofmann, K. Huber, R. Becker, D. C. Gregory, and E. Salzborn, J. Phys. B **20**, 1121 (1987).

[7] D. C. Gregory, P. F. Dittner, and D. H. Crandall, Phys. Rev. A **27**, 724 (1983).

[8] S. D. Loch, M. S. Pindzola, C. P. Ballance, D. C. Griffin, D. M. Mitnik, N. R. Badnell, M. G. O'Mullane, H. P. Summers, and A. D. Whiteford, Phys. Rev. A **66**, 052708 (2002).

[9] D. M. P. Holland, K. Codling, J. B. West, and G. V. Marr, J. Phys. B **12**, 2465 (1979).

[10] J. A. de Gouw, J. van Eck, A. Q. Wollrabe, J. van der Weg, and H. G. M. Heideman, J. Phys. B **27**, 3915 (1994).

[11] M. Lu, M. F. Gharaibeh, G. Alna'Washi, R. A. Phaneuf, A. L. D. Kilcoyne, E. Levenson, A. S. Schlachter, A. Müller, S. Schippers, J. Jacobi, S. W. J. Scully, and C. Cisneros, Phys. Rev. A **74**, 012703 (2006).

[12] A. M. Covington, A. Aguilar, I. R. Covington, M. F. Gharaibeh, G. Hinojosa, C. A. Shirley, R. A. Phaneuf, I. Álvarez, C. Cisneros, I. Dominguez-Lopez, M. M. Sant'Anna, A. S. Schlachter, B. M. McLaughlin, and A. Dalgarno, Phys. Rev. A **66**, 062710 (2002).

[13] Yu. Ralchenko, A. E. Kramida, J. Reader, A. E. Kramida, W. C. Martin, A. Musgrove, E. B. Saloman, C. J. Sansonetti, J. Reader, and J. J. Curry, URL: http://physics.nist.gov/cgi-bin/AtData/main_asd.
[14] G. C. King, M. Tronc, F. H. Read, and R. C. Bradford, J. Phys. B **10**, 2479 (1977).
[15] E. Hudson, D. A. Shirley, M. Domke, G. Remmers, A. Puschmann, T. Mandel, C. Xue, and G. Kaindl, Phys. Rev. A **47**, 361 (1993).
[16] R. Rejoub and R. A. Phaneuf, Phys. Rev. A **61**, 032706 (2000).
[17] M. Lu and R. A. Phaneuf, Phys. Rev. A **66**, 012706 (2002).
[18] M. Stenke, K. Aichele, D. Hathiramani, G. Hofmann, M. Steidl, R. Völpel, and E. Salzborn, Nucl. Instrum. Methods Phys. Res. B **98**, 573 (1995).
[19] M. F. Gu, *Atomic Processes in Plasmas*, edited by J. S. Cohen, S. Mazevet and D. P. Kilcrease, AIP Conf. Proc. No. **730** (AIP, New York, 2004), pp. 127–136; URL: http://kipac-tree.stanford.edu/fac/.
[20] R. D. Cowan, *The Theory of Atomic Structure and Spectra* (University of California Press, Berkeley, 1981).
[21] M. F. Gu, Astrophys. J. **590**, 113 (2003).
[22] E. D. Emmons, A. Aguilar, M. F. Gharaibeh, S. W. J. Scully, R. A. Phaneuf, A. L. D. Kilcoyne, A. S. Schlachter, I. Álvarez, C. Cisneros, and G. Hinojosa, Phys. Rev. A **71**, 042704 (2005).
[23] H. Kjeldsen, P. Andersen, F. Folkmann, J. Hansen, M. Kitajima, and T. Andersen, J. Phys. B **35**, 2845 (2002).
[24] W. Lotz, Z. Phys. **216**, 241 (1968).
[25] G. Hofmann, A. Muller, K. Tinschert, and E. Salzborn, Z. Phys. D: At., Mol. Clusters **16**, 113 (1990).
[26] T. W. Gorczyca, M. S. Pindzola, N. R. Badnell, and D. C. Griffin, Phys. Rev. A **49**, 4682 (1994).